Supporting Information

Ultra-stretchable Multilayered Fiber with a Hollow-Monolith Structure for High Performance Strain Sensor

Jiachen Gao, [1] *Xiaozheng Wang,* [1] *Wei Zhai,* [1] *Hu Liu,* [1] *Guoqiang Zheng,* [1] *Kun Dai,** [1] *Liwei Mi,* [2] *Chuntai Liu,* [1] *Changyu Shen* [1]

[1]School of Materials Science and Engineering, The Key Laboratory of Material Processing and Mold of Ministry of Education, Zhengzhou University, Zhengzhou, 450001, P. R. China

[2]Center for Advanced Materials Research, School of Materials and Chemical Engineering, Zhongyuan University of Technology, Zhengzhou, 450007, P. R. China

*E-mail: kundai@zzu.edu.cn

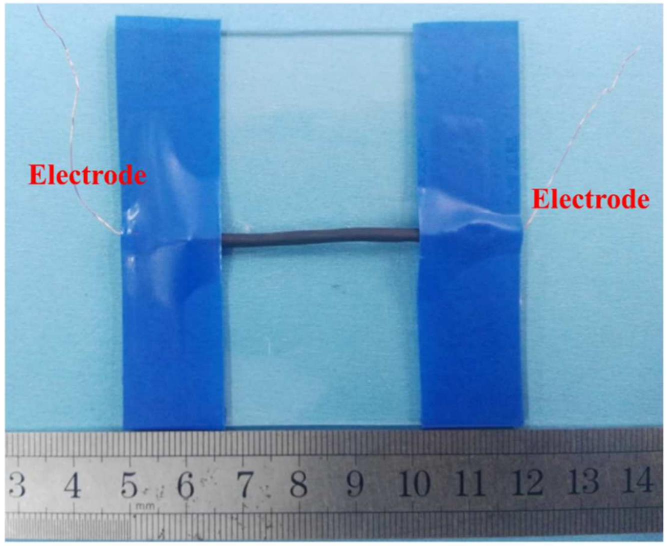

Figure S1. Photograph of the pressure sensor assembled by the TPU-8CNT@TPU fiber.

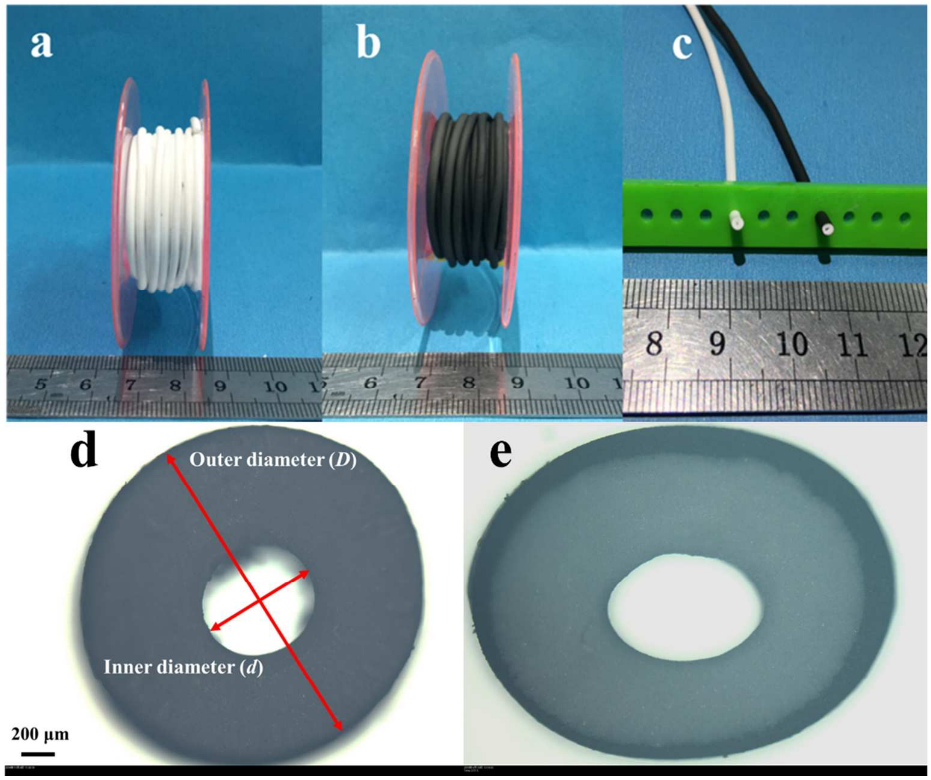

Figure S2. Digital photographs of (a) TPU-0CNT@TPU and (b) TPU-8CNT@TPU. (c) Comparison of cross section between TPU-0CNT@TPU (the white sample) and TPU-8CNT@TPU (the sample with a black shell). The POM images of (d) TPU-0CNT@TPU and (e) TPU-8CNT@TPU.

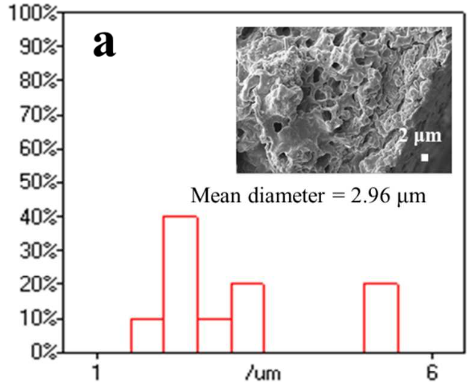

a. Diameter distribution of pores
in the outer layer of TPU-8CNT@TPU

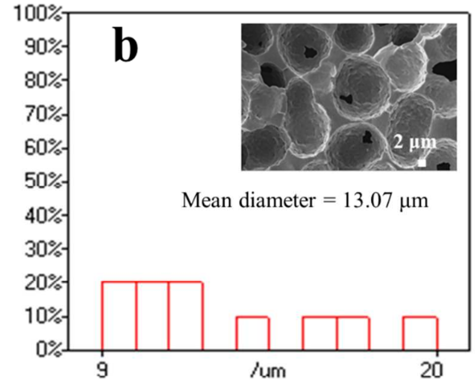

b. Diameter distribution of pores
in the inner layer of TPU-8CNT@TPU

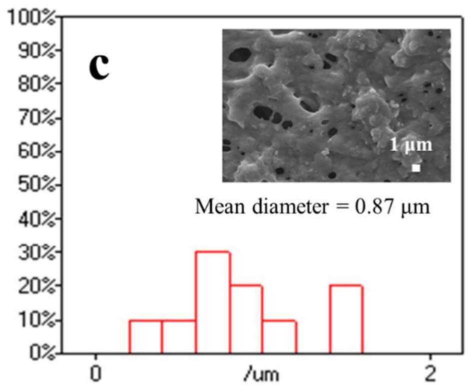

c. Diameter distribution of holes
in the surface of TPU-8CNT@TPU

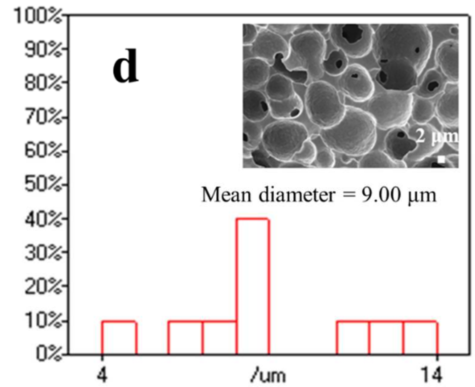

d. Diameter distribution of pores
of TPU-0CNT@TPU

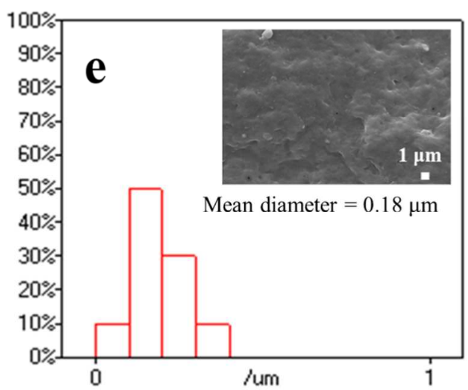

e. Diameter distribution of holes
in the surface of TPU-0CNT@TPU

Figure S3. Size distribution of pores or holes in different location of the fibers (the results are averaged at least ten measured values). Diameter distribution of (a) pores in the outer layer of TPU-8CNT@TPU; (b) pores in the inner layer of TPU-8CNT@TPU; (c) holes in the surface of TPU-8CNT@TPU; (d) pores of TPU-0CNT@TPU; (e) holes in the surface of TPU-0CNT@TPU.

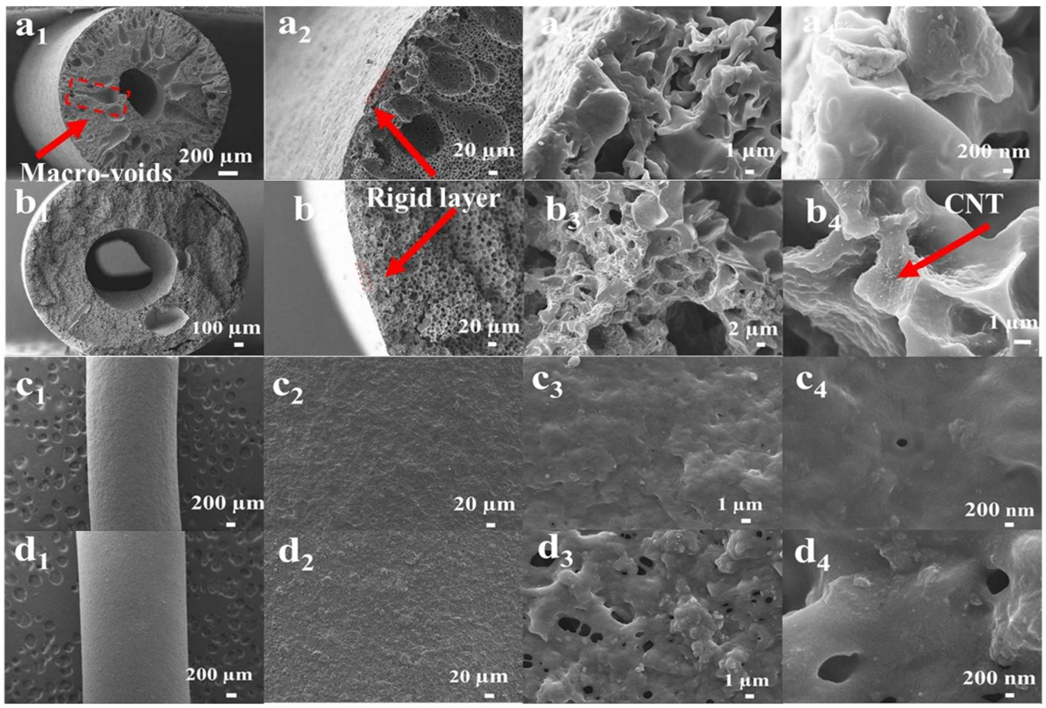

Figure S4. SEM images of the cross section of (a_1-a_4) TPU-0CNT@TPU, (b_1-b_4) TPU-8CNT@TPU, and surface of (c_1-c_4) TPU-0CNT@TPU, (d_1-d_4) TPU-8CNT@TPU at different magnifications.

1. The effect of the extrusion rate ratio of the outer layer to the inner layer on the fiber structure of TPU-8CNT@TPU.

In the experiment, the extrusion rate of the outer layer (defined as E_O) was 0.38 mL/min, and the inner layer extrusion rate (defined as E_I) was 1.09 mL/min, thus the extrusion rate ratio of the outer to inner (defined as $r = E_O/E_I$) was 0.34: 1. The fibers with varying r were fabricated under the same conditions. Interestingly, the results showed that the hollow structures of fibers disappeared when the r was 0 ($E_O = 0$ mL/min，Figure S5a) or infinity ($E_I = 0$ mL/min, Figure S5b). However, the fibers showed a denser cross section when the r was 0 than that was infinity. Specially, the fibers only possessed the monolith structure, while the hollow structure disappeared when the r was increased to 100: 1 (Figure S5c); it was impossible to prepare high quality wet-spun fibers when the r reduced to 0.05: 1 (Figure S5d). The effect of the r on the fibrous structure may mainly originate from two factors: one is the solidification rate of the fibers; the other is the die swell effect of the fiber affected by the shear rate in the spinning channel.[1] To prepare high quality sheath-core fibers with hollow and monolith structure, the spinning rate ratio of the spinning fiber must be controlled within a certain range (0.05:1 ~ 100:1). For example, the fibers showed multilayer-hollow-monolith structure when the r was 10:1 (Figure S5e) and 1:10 (Figure S5f).

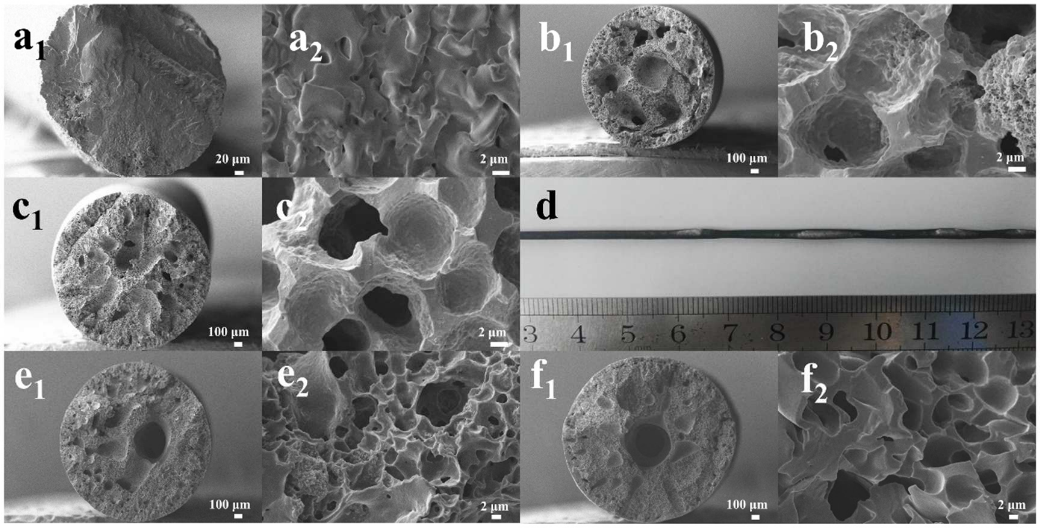

Figure S5. SEM images of cross section of TPU-8CNT@TPU with different r. (a_1-a_2) r = 0, (b_1-b_2) $r = \infty$, (c_1-c_2) r = 100:1, (e_1-e_2) r = 10:1, (f_1-f_2) r = 1:10 at different magnifications. (d) Digital photograph of the fiber with the r of 0.05:1.

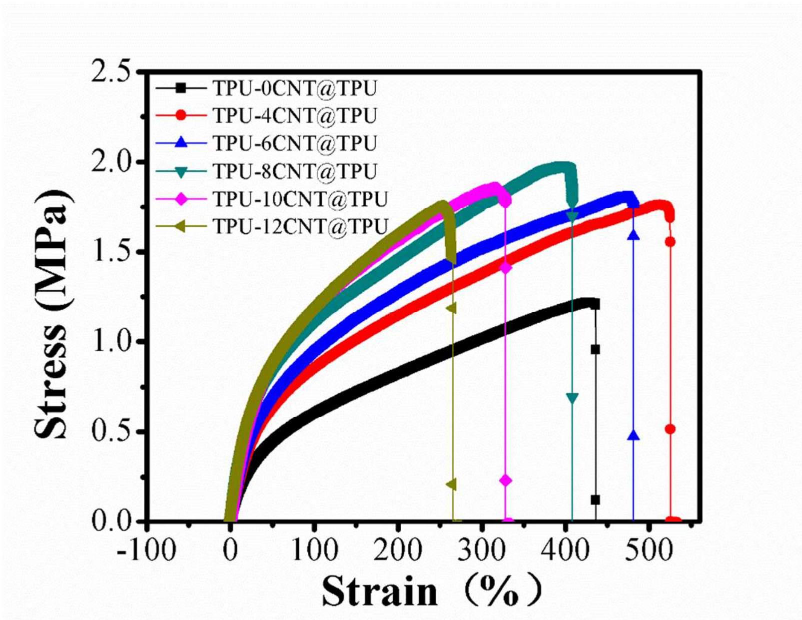

Figure S6. Typical stress vs. strain curves of the fibers with different CNTs loadings.

Table S1. Performance parameters of the fibers with different CNTs loadings.

	Breaking elongation	Strength (MPa)	Modulus (MPa)	Density (g/cm^3)
TPU-0CNT@TPU	4.32 ± 0.12	1.22 ± 0.057	1.44 ± 0.13	0.342 ± 0.0052
TPU-4CNT@TPU	4.76 ± 0.32	1.67 ± 0.099	1.86 ± 0.11	0.412 ± 0.0097
TPU-6CNT@TPU	4.44 ± 0.44	1.83 ± 0.077	2.34 ± 0.22	0.456 ± 0.024
TPU-8CNT@TPU	3.81 ± 0.31	1.86 ± 0.077	2.92 ± 0.45	0.464 ± 0.013
TPU-10CNT@TPU	3.19 ± 0.29	1.84 ± 0.093	3.04 ± 0.25	0.478 ± 0.019
TPU-12CNT@TPU	2.83 ± 0.26	1.79 ± 0.21	3.19 ± 0.34	0.513 ± 0.013

Note: the results are averaged at least five different fiber samples. The density is calculated using equation: $\rho = m/V$, where ρ, m and V are the density, mass, volume, respectively. The mass of the fibers was weighed by using a precision electronic balance (ESJ 182-4, Shenyang Shenyu Longteng Balance Co. Ltd., China).

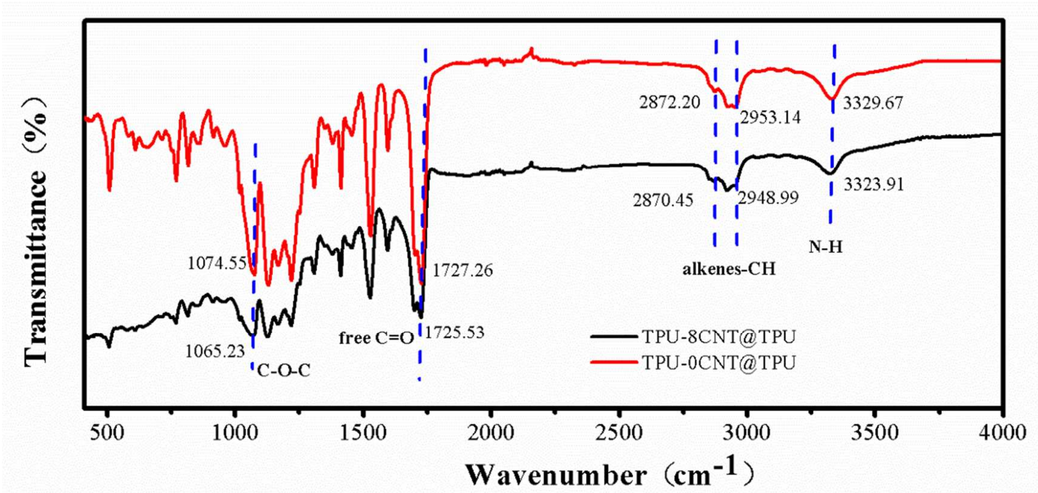

Figure S7. FTIR spectra of TPU-8CNT@TPU and TPU-0CNT@TPU (the spectrometer, Nicolet iS50). After the introduction of CNTs, several characteristic peaks of the fiber tend to be weaker and shift toward the low wavenumber, showing strong interactions between TPU polymer chains and CNTs.

Please see the references 2-4 on the discussions about the wavenumber of the corresponding functional groups.

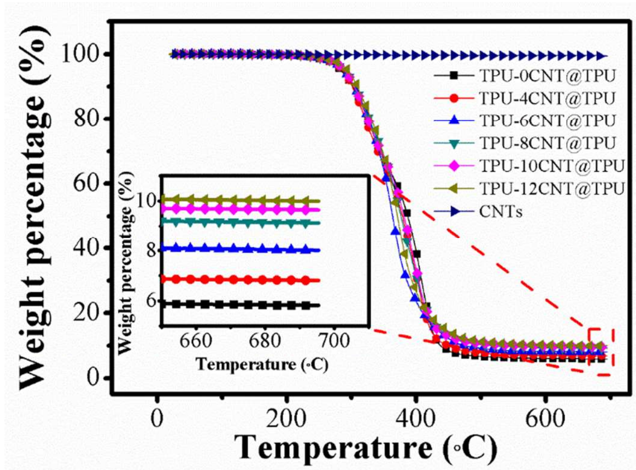

Figure S8. Thermogravimetric analysis (TGA) curves of CNTs and the fibers with different CNTs loadings. TGA was performed under a nitrogen atmosphere on a TGA/TA Q50 (TA Instruments Co., USA) from 30 to 700 ºC with a heating rate of 10 ºC/min.

Table S2. TGA results of CNTs and the fibers with different CNTs loadings.

Samples	Residue (wt.%)	ω_{CNTs} (wt.%)
TPU-0CNT@TPU	5.82	0
TPU-4CNT@TPU	6.81	0.99
TPU-6CNT@TPU	8.01	2.19
TPU-8CNT@TPU	9.13	3.31
TPU-10CNT@TPU	9.64	3.82
TPU-12CNT@TPU	9.99	4.17
CNTs	99.45	

Note : the mass fraction of CNTs in the whole fiber is calculated using equation: $\omega_{CNTs} = R_c - R_p$, where R_c, R_p and ω_{CNTs} represent the residual weight percentage of TPU-xCNT@TPU, TPU-0CNT@TPU at 700 ºC and the CNTs in the fibers.[2]

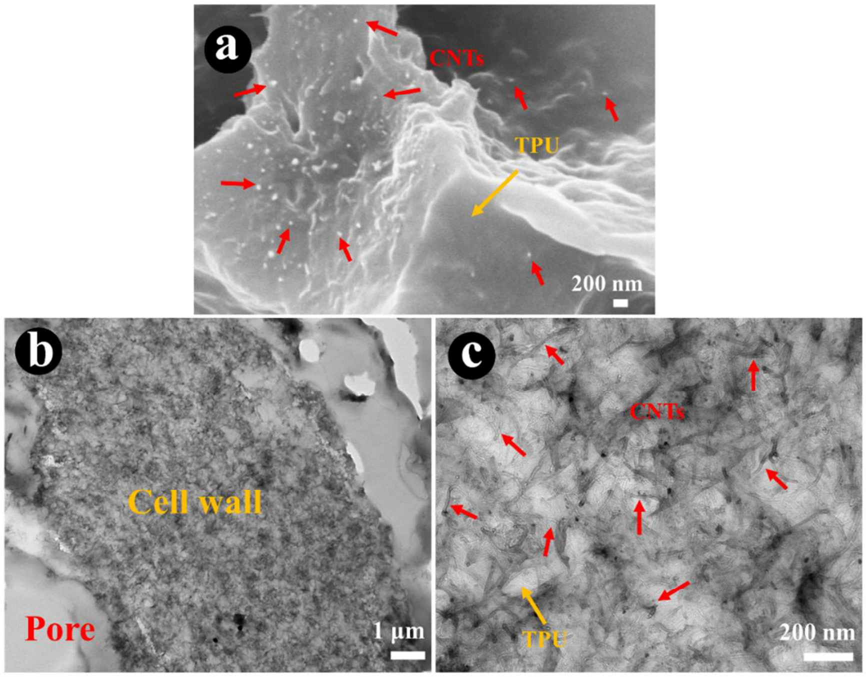

Figure S9. SEM (a) and TEM images (b), (c) of sensitive zone of TPU-8CNT@TPU.

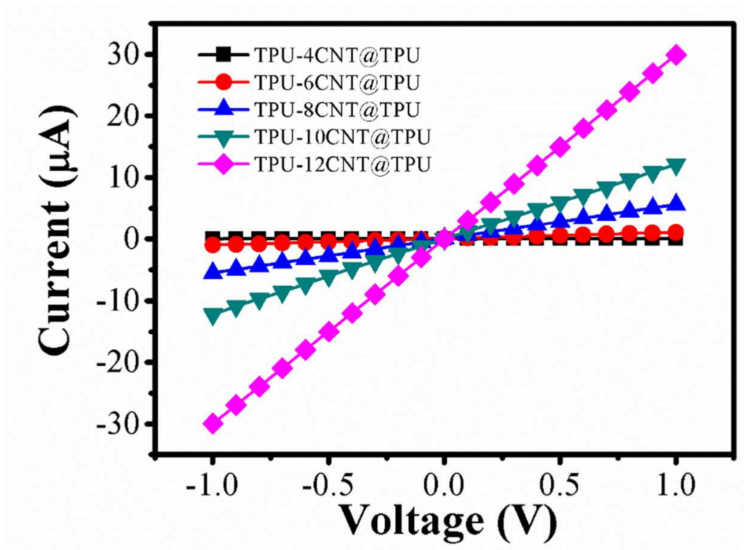

Figure S10. *I-V* characteristic curves of the fibers with different CNTs loadings (the electrochemical work station, RST5200F, Suzhou Risetest Electronic Co., Ltd., China).

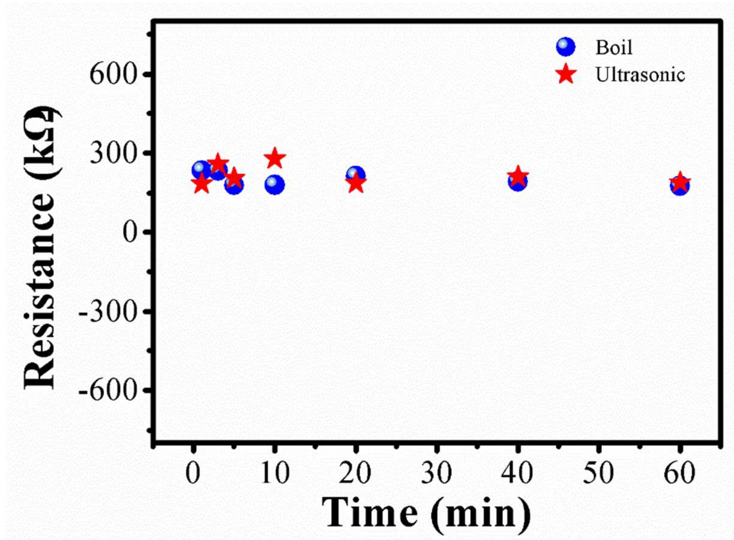

Figure S11. Change in *R* of the TPU-8CNT@TPU fiber as a function of ultrasonic and boiling time in deionized water to show the durability.

Table S3. The summary of maximum detection range and GF for typical flexible strain sensors reported in recent years.

Materials	Maximum detection range	GF	References
SWCNT/PU	60%	6.5	5
Hybrid SWCNTs/PEDOT:PSS/PU	100%	62	6
PEDOT:PSS/PVA	1.2%	396	7
MWCNTs/PU	400%	69	8
Graphene/PE	100%	≤ 10	9
Graphene/Nanocellulose fibril/PDMS	100%	7.1	10
Graphene sheets/ PDMS	7.5%	402.5	11
Carbonized silk fabric/Ecoflex	500%	37.5	12
CNTs/Lamellar layered double hydroxides	410%	12	13
SWCNTs/Cotton//PU	300%	0.65	14
Graphene/PVA	150%	1.33	15
MWCNT forest/PU	300%	1.07	16
MWCNT/TPU	350%	166.7	This work

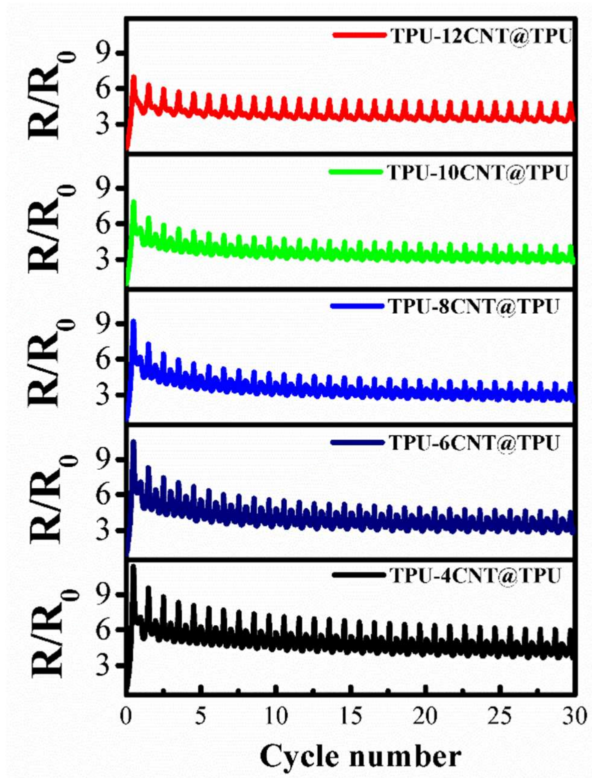

Figure S12. Change in R/R_0 of the fibers with different CNTs loadings under 80% strain at a rate of 50 mm/min during 1-30 cycles.

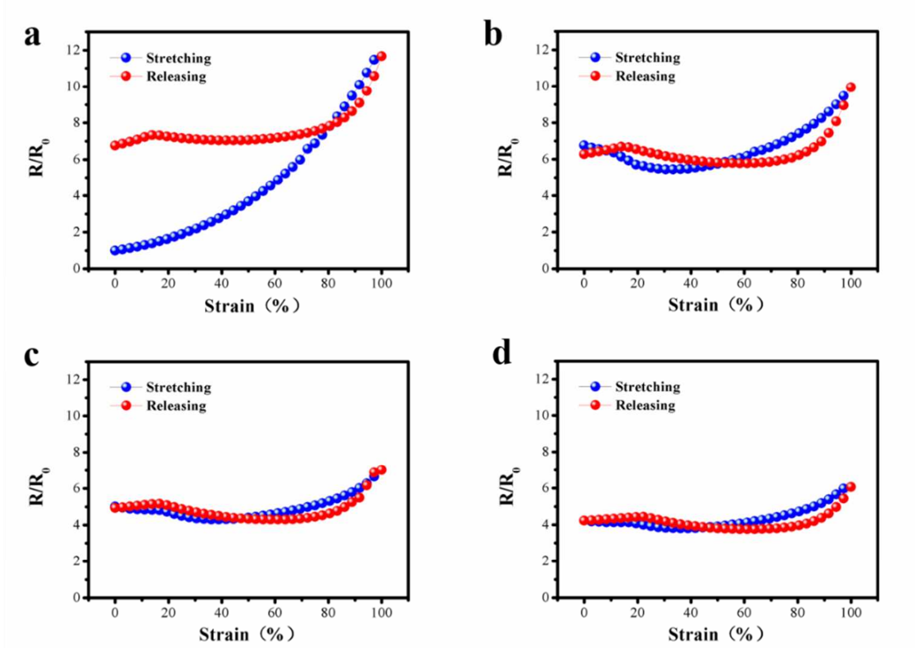

Figure S13. R/R_0-strain curves of TPU-8CNT@TPU for cyclic stretching-relaeasing tests: (a) 1st cycle, (b) 2nd cycle, (c) 10th cycle, (d) 30th cycle.

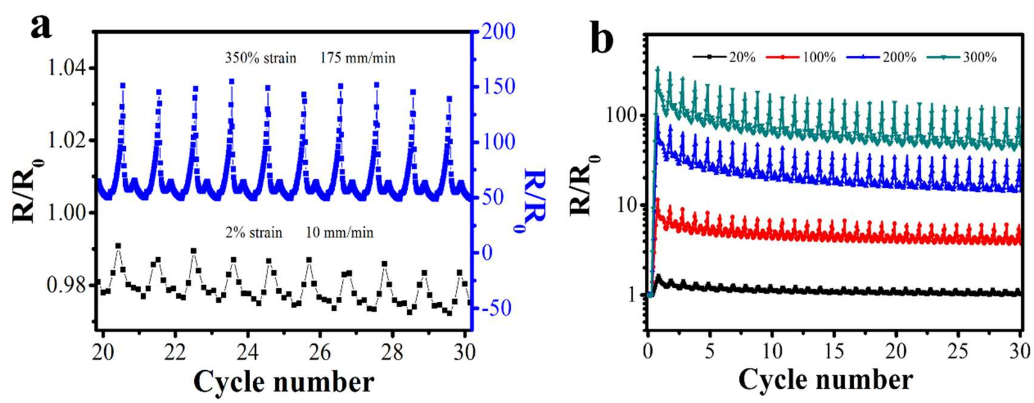

Figure S14. (a) Change in R/R_0 of TPU-8CNT@TPU under 2% and 350% strain during 21-30 cycles. (b) Change in R/R_0 of TPU-8CNT@TPU with the same frequency of 0.014 Hz at different strains during 1-30 cycles.

2. Determination of response time.

To calculate the strain response time, a step strain of 5% was applied at a rate of 500 mm/min for TPU-8CNT@TPU. The current response time of TPU-8CNT@TPU in the tensile process of 5% strain is defined as t_1 (Figure S12a), which is recorded by an electrochemical work station (RST5200F, Suzhou Risetest Electronic Co., Ltd., China), and tensile time of the tensile testing machine is defined as t_2, and the strain response time Δt_T is calculated as follows:

$$t_1 = 19.8508258 - 19.5037633 = 0.3470625 \text{ s}$$

$$t_2 = 30 \text{ mm} \times 5\% / (500 \text{ mm/min}) = 0.18 \text{ s}$$

$$\Delta t_T = t_1 - t_2 = 0.1670625 \text{ s} \approx 167 \text{ ms}$$

The compressive response time Δt_C is calculated by the same method, and a compression displacement of 1 mm is applied at the rate of 500 mm/min for TPU-8CNT@TPU (Figure S12b), the compressive response time Δt_C is calculated as follows:

$$t_1 = 17.2444816 - 17.0090301 = 0.2354515 \text{ s}$$

$$t_2 = (1 \text{ mm} / 500 \text{ mm/min}) = 0.12 \text{ s}$$

$$\Delta t_C = t_1 - t_2 = 0.1154515 \text{ s} \approx 115 \text{ ms}$$

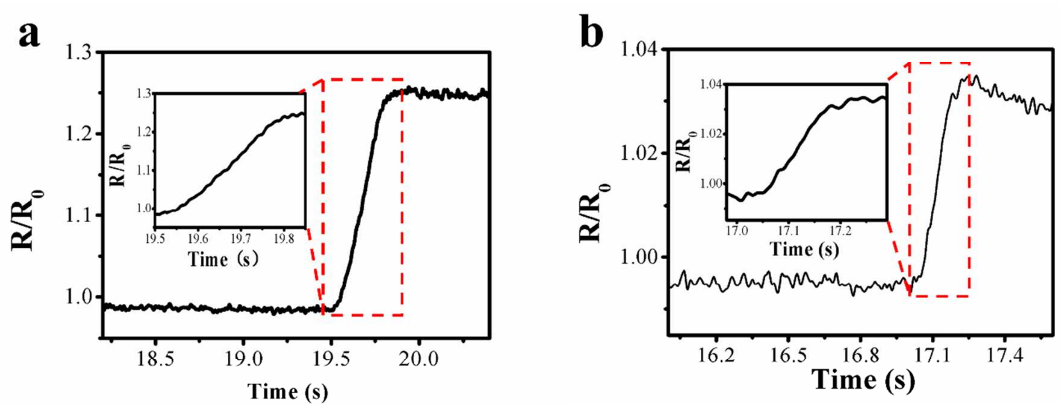

Figure S15. Response time of TPU-8CNT@TPU under (a) a step strain of 5% in tension and (b) 1 mm displacement at a strain rate of 500 mm/min in compression.

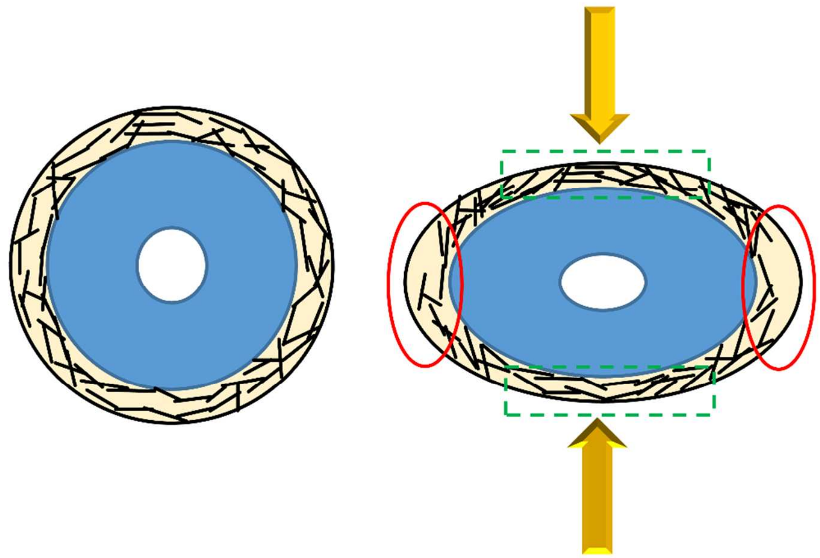

Figure S16. Schematic illustration of compression response mechanism.

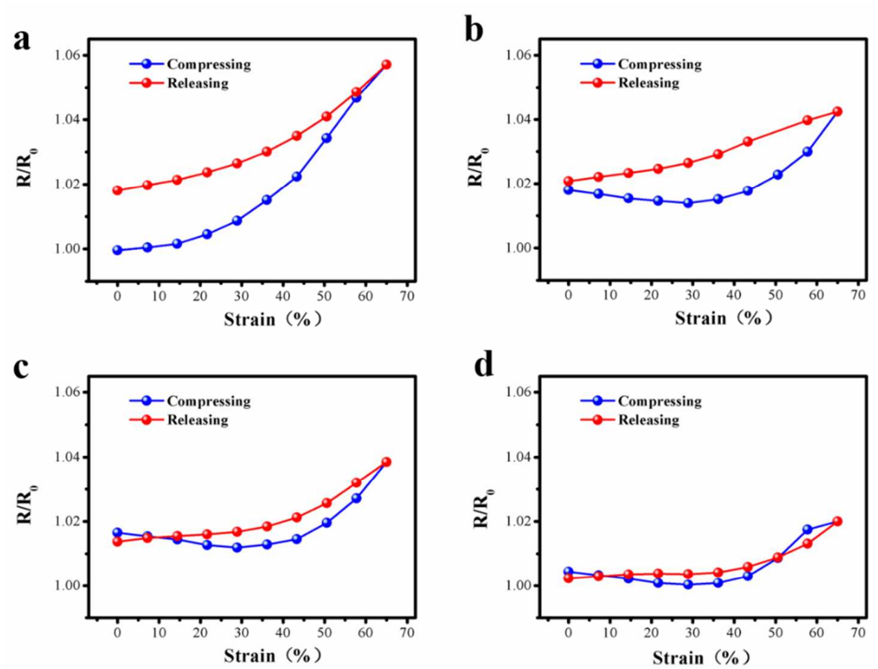

Figure S17. R/R_0-strain curves of TPU-8CNT@TPU for cyclic compressing-releasing tests: (a) 1st cycle, (b) 2nd cycle, (c) 4th cycle, (d) 10th cycle.

Table S4. Parameters obtained by fitting R/R_0 vs. strain curves with Equation (6) of TPU-8CNT@TPU in tension and compression, respectively.

	C	M	E	W	U	V
Tension	0.01201	0.60455	127.75779	0.33129	-0.23464	0.0322
Compression	0.00446	-0.21202	46.57262	-0.07359	0.36182	-0.16917

REFERENCES

(1) Ishigami, T.; Kasuya, Y.; Rajabzadeh, S.; Ohmukai, Y.; Kakihana, Y.; Matsuyama, H., Effect of Solidification Rate of Polymer Solution on the Die-Swell during Hollow Fiber Spinning by Non-Solvent Induced Phase Separation. *J. Membr. Sci.* **2014,** *472*, 194-201.

(2) Guan, X.; Zheng, G.; Dai, K.; Liu, C.; Yan, X.; Shen, C.; Guo, Z., Carbon Nanotubes-Adsorbed Electrospun PA66 Nanofiber Bundles with Improved Conductivity and Robust Flexibility. *ACS Appl. Mater. Interfaces* **2016,** *8*, 14150-14159.

(3) Li, Y.; Zhou, B.; Zheng, G.; Liu, X.; Li, T.; Yan, C.; Cheng, C.; Dai, K.; Liu, C.; Shen, C.; Guo, Z., Continuously Prepared Highly Conductive and Stretchable SWNT/MWNT Synergistically Composited Electrospun Thermoplastic Polyurethane Yarns for Wearable Sensing. *J. Mater. Chem. C* **2018,** *6*, 2258-2269.

(4) Wang, Y.; Hao, J.; Huang, Z.; Zheng, G.; Dai, K.; Liu, C.; Shen, C., Flexible Electrically Resistive-Type Strain Sensors Based on Reduced Graphene

Oxide-Decorated Electrospun Polymer Fibrous Mats for Human Motion Monitoring. *Carbon* **2018,** *126*, 360-371.

(5) Seyedin, S.; Razal, J. M.; Innis, P. C.; Wallace, G. G., A Facile Approach to Spinning Multifunctional Conductive Elastomer Fibres with Nanocarbon Fillers. *Smart Mater. Struct.* **2016,** *25*, 035015.

(6) Roh, E.; Hwang, B. U.; Kim, D.; Kim, B. Y.; Lee, N. E., Stretchable, Transparent, Ultrasensitive, and Patchable Strain Sensor for Human-Machine Interfaces Comprising A Nanohybrid of Carbon Nanotubes and Conductive Elastomers. *ACS Nano* **2015,** *9*, 6252-6261.

(7) Liu, N.; Fang, G.; Wan, J.; Zhou, H.; Long, H.; Zhao, X., Electrospun PEDOT:PSS–PVA Nanofiber Based Ultrahigh-Strain Sensors with Controllable Electrical Conductivity. *J. Mater. Chem.* **2011,** *21*, 18962-18966.

(8) Slobodian, P.; Riha, P.; Benlikaya, R.; Svoboda, P.; Petras, D., A Flexible Multifunctional Sensor Based on Carbon Nanotube/Polyurethane Composite. *IEEE Sens. J.* **2013,** *13*, 4045-4048.

(9) Cheng, Y.; Wang, R.; Sun, J.; Gao, L., A Stretchable and Highly Sensitive Graphene-Based Fiber for Sensing Tensile Strain, Bending, and Torsion. *Adv. Mater.* **2015,** *27*, 7365-7371.

(10) Yan, C.; Wang, J.; Kang, W.; Cui, M.; Wang, X.; Foo, C. Y.; Chee, K. J.; Lee, P. S., Highly Stretchable Piezoresistive Graphene-Nanocellulose Nanopaper for Strain Sensors. *Adv. Mater.* **2014,** *26*, 2022-2027.

(11) Wang, D. Y.; Tao, L. Q.; Liu, Y.; Zhang, T. Y.; Pang, Y.; Wang, Q.; Jiang, S.; Yang,

Y.; Ren, T. L., High Performance Flexible Strain Sensor Based on Self-Locked Overlapping Graphene Sheets. *Nanoscale* **2016,** *8*, 20090-20095.

(12) Wang, C.; Li, X.; Gao, E.; Jian, M.; Xia, K.; Wang, Q.; Xu, Z.; Ren, T.; Zhang, Y., Carbonized Silk Fabric for Ultrastretchable, Highly Sensitive, and Wearable Strain Sensors. *Adv. Mater.* **2016,** *28*, 6640-6648.

(13) Li, C.; Cui, Y. L.; Tian, G. L.; Shu, Y.; Wang, X. F.; Tian, H.; Yang, Y.; Wei, F.; Ren, T. L., Flexible CNT-Array Double Helices Strain Sensor with High Stretchability for Motion Capture. *Sci. Rep.* **2015,** *5*, 15554.

(14) Wang, Z.; Huang, Y.; Sun, J.; Huang, Y.; Hu, H.; Jiang, R.; Gai, W.; Li, G.; Zhi, C., Polyurethane/Cotton/Carbon Nanotubes Core-Spun Yarn as High Reliability Stretchable Strain Sensor for Human Motion Detection. *ACS Appl. Mater. Interfaces* **2016,** *8*, 24837-24843.

(15) Park, J. J.; Hyun, W. J.; Mun, S. C.; Park, Y. T.; Park, O. O., Highly Stretchable and Wearable Graphene Strain Sensors with Controllable Sensitivity for Human Motion Monitoring. *ACS Appl. Mater. Interfaces* **2015,** *7*, 6317-6324.

(16) Shin, M. K.; Oh, J.; Lima, M.; Kozlov, M. E.; Kim, S. J.; Baughman, R. H., Elastomeric Conductive Composites Based on Carbon Nanotube Forests. *Adv. Mater.* **2010,** *22*, 2663-2667.